18th IMEKO TC10 Conference
"Measurement for Diagnostics, Optimisation and Control to Support Sustainability and Resilience"
Warsaw, Poland, September 26–27, 2022

Identification of Defects in the Magnetoelectric Ring Sensor using Spectral Analysis

Karol Kuczynski[1], Piotr Bilski[2], Adrian Bilski[3], Jerzy Szymanski[1]

[1] *Kazimierz Pulaski University of Technology and Humanities in Radom, Faculty of Transport, Electrical Engineering and Computer Science, Poland; k.kuczynski@uthrad.pl; j.szymanski@uthrad.pl*
[2] *Warsaw University of Technology, Faculty of Electronics and Information Technology, Institute of Radioelectronics and Multimedia Technology, Poland; piotr.bilski@pw.edu.pl*
[3] *Warsaw University of Life Sciences, Poland, adrian_bilski@sggw.edu.pl*

***Abstract* – The paper discusses the method for detecting defects that may arise in the construction of ring-shaped magnetoelectric sensors. The approach is based on the amplitude and phase spectral analysis generated on the sensor's output. The defect detection is performed using the Discrete Fourier Transform (DFT). The experiments covered two faults, related to the physical dislocation of the amorphous metal ribbon around the magnetic ring. Results show that it is possible to automatically locate particular defects in the electromagnetic sensor based on the input-output characteristic analysis**

Keywords – ring magnetoelectric sensor, DFT, defects.

I. INTRODUCTION

Electromagnetic sensors are demanding instruments for monitoring and diagnostics. Their state influences readings of the measured quantity. The operating regime of the sensor consists in presenting the AC signal-based on the state of the magnetic field. Unfortunately, the measurement results are affected by the physical defects in the instrument construction, such as the geometric size of the amorphic metal ribbon, which is the core element of the sensor. It is then important to know the actual state of the device (for example to be used during the sensor's calibration).

The sensor considered in the paper can be used for detecting the constant components of the magnetic field, even of the low magnitude. Its circular shape makes it also usable for energy harvesting, which is a hot topic due to the growing importance of the green technologies. Multiple sensors located around the traction line of the train or tram can be used to extract energy from the power lines. However, their efficiency strongly depends on the condition of each device. This justifies proposing the diagnostics scheme allowing for the on-line monitoring of the actual sensor's state.

Because of the system's complexity, it is important to apply the precisely crafted method, adjusted for its specific structure and work regime. The obvious choice today is application of the soft computing approach. There are multiple fault identification methods for that purpose [1-6]. Artificial Intelligence (AI)-based methods are popular due to their high flexibility, combined with the ability to automatically extract knowledge, required for subsequent decision making [7, 8]. Their efficiency, however, depends on the meticulous selection of the features that would be extracted from the recorded signals [1].

The paper presents the diagnostic approach to determine the defects in the magnetoelectric ring sensor, which is the original construction of the authors. Two scenarios were selected to show the relation between the state of the sensor and its responses for known excitation (i.e. known magnetic field). The fault identification is based on the spectral analysis of the voltage induced by the sensor as the response to the magnetic field's strength in the vicinity of the device.

The paper is organized as follows. In Section II the analysed sensor is introduced. Section III presents the experimental setup (as the whole diagnostic procedure was performed on the actual device) with the diagnostic procedure. Experimental results are in Section IV, while conclusions with future prospects are in Section V.

II. MAGNETOELECTRIC (ME) RING SENSOR

Over the years, many solutions of magnetoelectric magnetic field sensors have been constructed [9-11]. In the systems presented in [12], the voltage induced in the sensor at the output of the piezoelectric electrodes, which was excited by a constant magnetic field, was linearly dependent on the measured alternating magnetic field.

On the other hand, current transducers made of ME composites enable the measurement of AC or DC current flowing in a conductor by measuring the AC or DC eddy

magnetic field excited around this conductor in accordance with the Ampere's law. The magnetic field's strength depends on the value of the current I in the conductor and the distance r from this conductor.

$$H = I/2\pi r, \qquad (1)$$

Therefore ME ring laminates are essential for electrical current sensors [13, 14]. For example, in a ring electric current sensor was presented, which reacts to an eddy magnetic field. The sensor's design was based on an axially polarized PZT ceramic ring, sandwiched between two circumferentially magnetized composite rings composed of an epoxy resin Terphenol-D / NdFeB magnet.

The Metglas / Piezoelectric (PZT) laminates are often used to construct such sensors [15, 16]. They form an open or closed magnetic circuit (OMC and CMC) of various widths (W), lengths (L) and diameters (D). Among these geometries, CMC laminates have advantages not only in terms of magnetic flux distribution, but also sensitivity and independence from the position of the vortex center. The ME voltage signal is enhanced by increasing the volume of the magnetostrictive phase by using four layers of Metglas metal ribbon. [16].

The sensor used to the measured DC magnetic strength in the presented research [17] is built of a thin-walled ring (1) made of PZT piezoelectric ceramics with a height approximately equal to half the outer diameter (Figure 1). The piezoelectric ceramics are characterized by high values of the dielectric constant, piezoelectric constant and piezoelectric voltage ratio. On the outer surface of the ring (1) there is centrally glued amorphous ribbon (2) with a width twice smaller than the height of the ring (1). The ribbon (2) has a narrow magnetic hysteresis loop, thanks to which it has low energy losses needed to remagnetize the material. The ribbon (2) is connected to the ring (1) used for gluing the strain gauges. The excitation winding (3) is wound on the ring (1) combined with the strip (2). An exciting current I_s is applied to the winding (3), which creates an alternating excitation field H_s, which stimulates the sensor to operate. A constant, measured magnetic field H_{dc} acts on the ribbon (2) attached to the ring (1), which causes a magnetostrictive deformation in the ribbon (2) which is transferred to the piezoelectric ring (1). As a result of the influence of the H_{dc} field on the electrodes at the edges of the ring (1), the voltage U_{dc} is generated, proportional to the value of H_{dc}, and the comparison of the field with the measured voltage U_{dc} is the measurement result [17, 18].

During the tests of prototypes, it was found that due to the aging effects the air gap between magnetostictive metall ribbon and piezoelectric emerges. The second problem is the occurrence of the magnetic hysteresis loop, which is the defect, degrading, for instance the energy harvesting efficiency. To detect both types of faults, the diagnostic procedure was proposed.

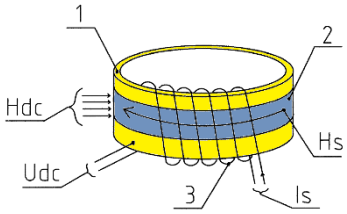

Fig. 1. Diagram of the magnetoelectric magnetic field sensor used during the research [17]

III. EXPERIMENTAL SETUP

The measuring system for analyzing the sensor output voltage is shown in Figure 2. It consists of: the pickup coil producing an exciting magnetic field of the analyzed device, magnetoelectric ring sensor and the digital measuring system. The exciting field is driven by the current generator working at 1kHz (which is the standard frequency for testing material properties of such sensors, including relative dielectric constant and dielectric dissipation factor [19]). The output signal from the sensor is a function of the measured constant magnetic field H_{dc}. It is processed by the measuring system containing the digital oscilloscope DS1054Z and TDS1002B connected to the PC [20].

The system allows for the visualization of the magnetoelectric field sensor characteristics. These system enable evaluating U_{out} in the function of the measured constant magnetic field H_{dc} with additional value of H_s function:

$$H_s = U_m \cdot sin(\omega t), \qquad (2)$$

where U_m is proportional to the amplitude of the current created in the magnetic field control system.

The following testing scenario was proposed. The sensor is excited with the alternate magnetic field H_s of known magnitude and direction. The voltage induced by it is then recorded and processed by the diagnostic module. Based on the symptoms extracted from the signals in time and frequency domain, the size of the gap is evaluated through the DFT-based module. The signal processing software was prepared in the Python language.

To determine the state of the sensor (and detect the air gap), the recorded voltage patterns are processed in order to find the features, being either the characteristic points in the sinusoidal pattern, or harmonics in the spectrum. The DFT analysis was used to find the differences in the output waveforms from the sensor. Comparison of spectra is done through generation of the residual pattern being the difference between the nominal and actual vectors of spectral samples. Though the defect is also visible in the time domain, for the automated procedure it is easier to perform operations on spectral samples (assuming

identical DFT parameters through the whole operation).

Currently the proposed approach treats faults as catastrophic, i.e. changing the topology of the sensor. In the future, when more devices will be constructed and more defects generated, it will be possibile to introduce parameteric faults, where each defect will have different intensity, also detectable.

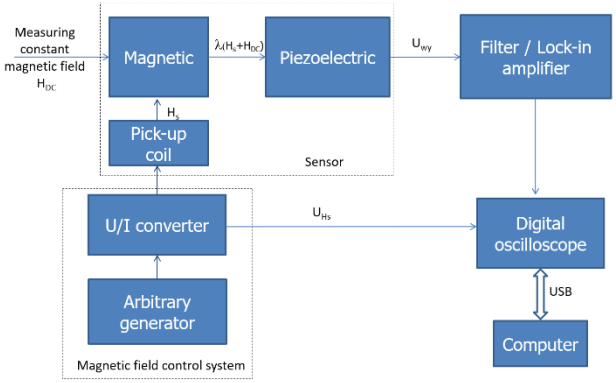

Fig. 2. Schematic block diagram of the measuring system.

IV. RESULTS AND DISCUSSIONS

The experiments were conducted using multiple sensors of identical design, differing in geometrical sizes. Parameters of the tested prototypes are presented in Table 1. Their geometrical sizes are significantly different and were selected to demonstrate two problems found in the prototypes. In the P1 sensor there was the air gap that occurred after a couple of months of the device operation. In the sensor P2 the hysteresis loop emerges, which is considered an unwanted effect, as it makes taking measurements more difficult. The procedure operation is illustrated in subsequent figures, though in the practical application only the result of the processing is given to the user (i.e. information about the state of the sensor).

Table 1. Parameters of the tested prototypes

sample	outer diameter, [mm]	inner diameter [mm]	ring height, [mm]	PZT	amorphous ribbon
P1	78	64	35	K2	$Fe_{78}B_{13}Si_9$
P2	24	20	15	PZ27	Metglas 2605Co

A. Prototype P1

This prototype consists of a K2 piezoelectric ring by Cerad and 1 coil of amorphous ribbon glued to the outer diameter of the piezoelectric ring. To demonstrate the fault detection procedure, first its nominal operation is presented (Fig. 3 to 5), then the faulty state is illustrated (Fig. 6 to 8).

Fig. 3 shows the recorded excitation field H_s (green pattern) and the corresponding output voltage U_{out} (red pattern). Fig. 4 shows the amplitude spectrum of the U_{out} output signal, while Fig. 5 presents its phase spectrum. The output waveform from the sensor was reconstructed by summing up the sinusoids with amplitudes equal to the harmonic values for individual frequencies, taking into account their phase shifts. This was to check the correctness of the applied DFT algorithm. The energy of the correct signal is located in the low part of the spectrum (below10 kHz), there is no hysteresis visible, though the high-frequency components of low magnitude can be observed (at tens or even hundreds of kHz). The phase spectrum is uniform for all frequencies.

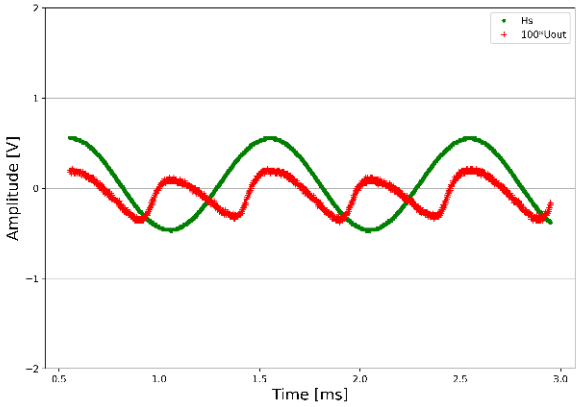

Fig. 3. Voltage waveform in the sensor's output from prototype P1 before the defect (nominal state).

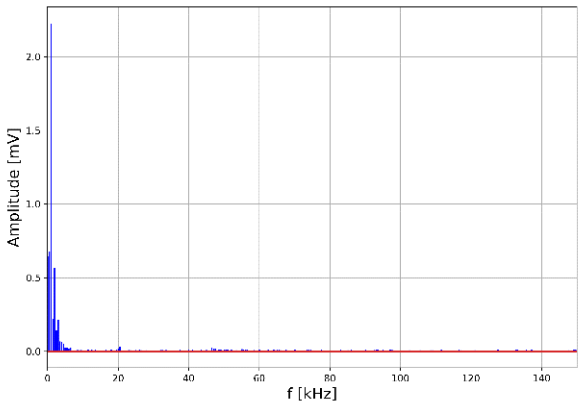

Fig. 4. Amplitude spectrum from voltage waveform in the sensor's output from prototype P1 before the defect (nominal state).

In the case of the fault, the air gap is present, which changes the signal, both in the time (Figure 6) and the frequency domain (Figure 7 and 8). The red-coloured sinusoidal pattern obtains now medium frequency component, added to the waveform and independent of the high frequency noise (which is present even in the nominal state). A better view of the change is in the amplitude spectrum, where additional components of relatively high energy are present at around 14kHz. On the other hand, though the phase spectrum also bears the difference from the nominal pattern, its interpretation is more difficult and should be investigated further.

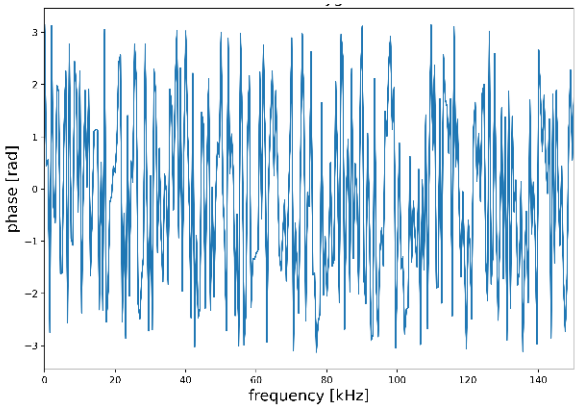

Fig. 5. Phase spectrum from voltage waveform in the sensor's output from prototype P1 before the defect.

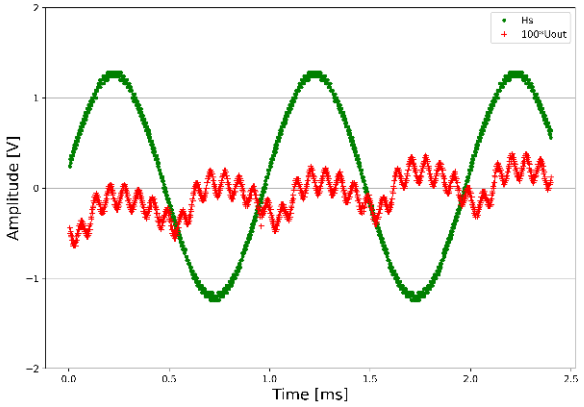

Fig. 6. Voltage waveform in the sensor's output from prototype P1 during the defect manifestation.

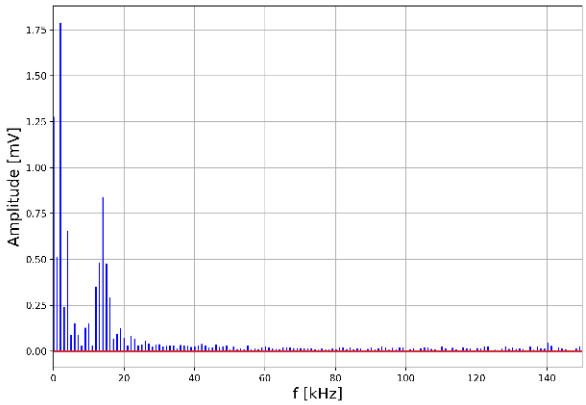

Fig. 7. Amplitude spectrum from voltage waveform in the sensor's output from prototype P1 during the defect manifestation.

Figure 9 shows the difference in harmonic values of the undamaged sensor from the damaged one. Initial changes with the opposite sign result from the inaccuracy of the method and measurements in two different laboratory rooms. At the particular range of frequencies there are non-zero values, indicating fault of the sensor.

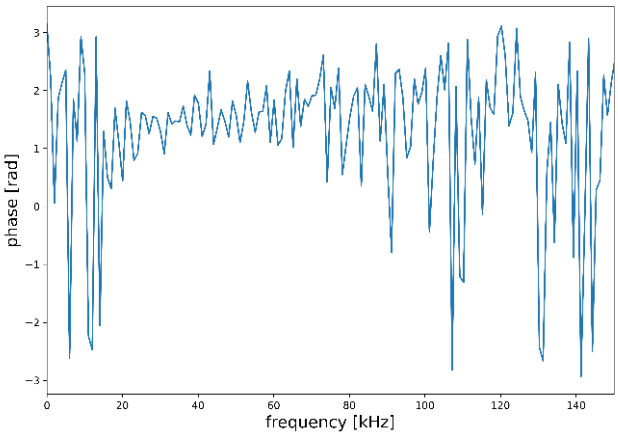

Fig. 8. Phase spectrum from voltage waveform in the sensor's output from prototype P1 during the defect manifestation.

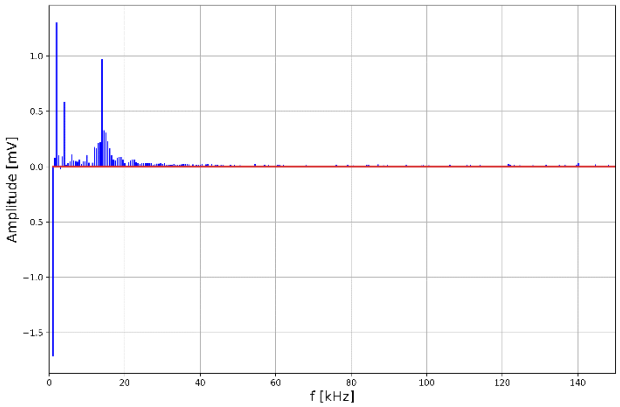

Fig. 9. Differential Amplitude spectrum from voltage waveform in the sensor's output from prototype P1 during the defect manifestation and without dfect.

B. Prototype P2

The P2 prototype consists of a PZT 27 ring and 1 coil of amorphous 2605Co ribbon glued to the outer diameter of the piezoelectric ring. In this case the problem is the hysteresis loop that is visible even in the single measurement in the time domain. Fig. 10 shows the recorded waveforms of the H_s excitation field and the output voltage U_{out}. The red envelope is the unwanted effect that emerged after utilization of the device.

Fig. 11 shows the amplitude, while Fig. 12 – phase spectrum of the U_{out} output signal. Again, Fig. 11 is the most informative, as multiple frequency components between 14 and 150kHz are present. Unfortunately, the phase is difficult to interpret and is less different from the nominal state than in the case of the air gap.

Based on the conducted experiments it is visible that the spectral analysis of the sensor's output voltage is the useful tool for detecting selected defects in the device. The proposed approach is semi-automated, i.e. the residual spectrum is obtained automatically, but the decision about the state of the sensor must be made manually, by the

human expert. Besides, the spectrum-based approach is best suited for analysing the time-invariant signals, as short and abrupt changes will not be visible.

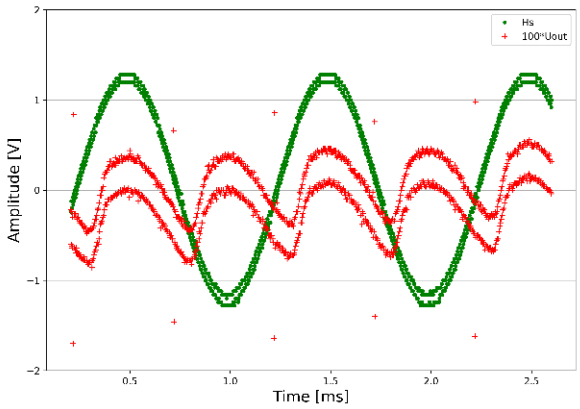

Fig. 10. Voltage waveform in the sensor's output from prototype P2 during the defect occurrence.

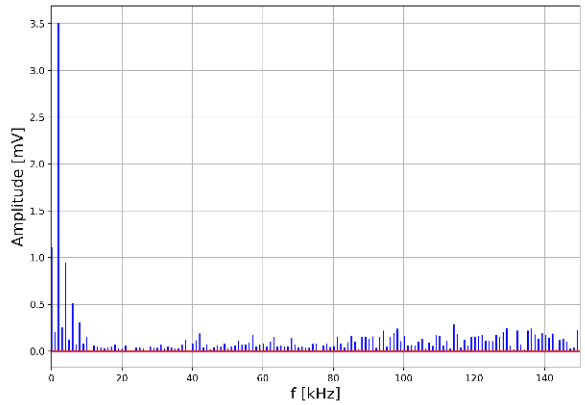

Fig. 11. Amplitude spectrum from voltage waveform in the sensor's output from prototype P2 during the defect occurrence.

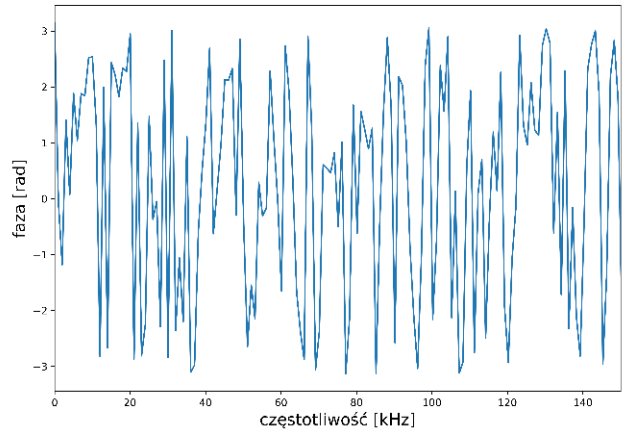

Fig. 12. Phase spectrum from voltage waveform in the sensor's output from prototype P2 during the defect occurrence.

After additional research it is expected to produce knowledge (for instance, in the form of rules) that would help to automate process. Application of AI-based approaches requires more data for machine learning, i.e. more sensors and measurements.

V. CONCLUSIONS

The conducted research shows the potential of the spectral analysis to determine the actual state of the electromagnetic sensor. It may be used to periodically test devices in order to determine whether they are wearing out. Experiments on two prototypes with two different defects show that the fault is visible in higher frequencies of the amplitude spectrum (which is the easiest for the automated extraction of features to create the residual signal). In the case of the sensor P1 the problem suffered from possible aging effects of the adhesive. Where the glue aged faster, an air gap was created between the piezoelectric ring and the amorphous ribbon. In the P2 prototype a wide magnetic hysteresis loop manifests. The analysis phase spectrum leads to ambiguous conclusions and should be focused on in the incoming works.

The next step of the research will be implementation of the AI-based approach to perform the whole diagnostic procedure automatically. For that purpose more devices must be assembled with different defects of the varying intensity. This way it will be possible to train the classifier based on multiple examples (spectral components extracted from measured signals). We have to use the following classical neural networks (NN), including multilayer perceptrons (MLP) or deep neural networks (DNN) as well Clasiffication Trees [2, 21].

VI. ACKNOWLEDGMENTS

We would like to thank prof. Aleksandra Kolano-Burian from Łukasiewicz Research Network - Institute of Non-Ferrous Metals for supply of the $Fe_{78}B_{13}Si_9$ components used in this study.

REFERENCES

[1] W. Hochwald and J.D. Bastian, "A DC Dictionary Approach for analog Fault Dictionary Determination," IEEE Trans. Cir. Syst., vol. 26, 1979, pp. 523-529.

[2] P. Pietrzak, M. Wolkiewicz and T. Orlowska-Kowalska, "PMSM Stator Winding Fault Detection and Classification Based on Bispectrum Analysis and Convolutional Neural Network," in IEEE Transactions on Industrial Electronics, 2022, doi: 10.1109/TIE.2022.3189076.

[3] P. Bilski and J. Wojciechowski, "Automated Diagnostics of Analog Systems Using Fuzzy Logic Approach," IEEE Trans. Instrum. Meas., vol. 56, no. 6, 2007, pp. 2175-2185.

[4] P. Wang and S. Yang, "A New Diagnosis Approach for Handling Tolerance in Analog and Mixed-Signal Circuits by Using Fuzzy Math," IEEE Trans. Cir. Syst.-I., vol. 53, no. 10, 2005, pp. 2118-2127.

[5] M. Aminian and F. Aminian, "A Modular Fault-Diagnostic System for Analog Electronic Circuit Using Neural Networks With Wavelet Transform as a Preprocessor," IEEE Trans. Instrum. Meas., vol. 56, no. 5, 2007, pp. 1546-1554.

[6] T. Gao, J. Yang, J. Wang and S. Jiang, "A Novel Fault Detection Method Based on Multiple Features for Analog Circuits," 2021 Global Reliability and Prognostics and Health Management (PHM-Nanjing), 2021, pp. 1-8, doi: 10.1109/PHM-Nanjing52125.2021.9612952..

[7] P. Bilski, "Automated selection of kernel parameters in diagnostics of analog systems," Electr. Rev., vol. 87, no. 5, 2011, pp. 9-13.

[8] T. Hastie, R. Tibshirani, J. Friedman, The Elements of Statistical Learning: Data Mining, Inference, and Prediction. 2nd ed., Springer, 12th printing with corrections, Jan 2017, [Online]. Available: http://statweb.stanford.edu/~tibs/ElemStatLearn/ [Accessed: 10. Jun. 2022].

[9] M. Bichurin, R. Petrov, O. Sokolov, V. Leontiev, V. Kuts, D. Kiselev, Y. Wang, "Magnetoelectric Magnetic Field Sensors: A Review," Sensors, vol. 21, pp. 6232, 2021, doi:10.3390/s21186232.

[10] C. M. Leung, J. Li, D. Viehland, X. Zhuang, "A review of applications of magnetoelectric composites: from heterostructural uncooled magnetic sensors to energy harvesters to highly efficient power converters," Journal of Physics D: Applied Physics, vol. 51, 2018, doi: 10.1088/1361-6463/aac60b.

[11] F. Narita, M. A. Fox, "Review on Piezoelectric, Magnetostrictive, and Magnetoelectric Materials and Device Technologies for Energy Harvesting Applications," Advanced Engineering Materials, vol. 20, 2018, doi:10.1002/adem.201700743.

[12] G. Srinivasan, S. Priya, N. X. Sun, Composite Magnetoelectrics - Materials, Structures, and Applications, Woodhead Publishing Series in Electronic and Optical Materials: Number 62, Elsevier, 2015.

[13] S. Priya, R. Islam, S. Dong, D. Viehland, Recent advancements in magnetoelectric particulate and laminate composites, J. Electroceram 19, 2007, s.147–164.

[14] H. Palneedi, V. Annapureddy, S. Priya, J. Ryu, "Status and Perspectives of Multiferroic Magnetoelectric Composite Materials and Applications," Actuators, vol. 5, 2016, doi: 10.3390/act5010009.

[15] D. Xie, Y. Wang, J. Cheng, "Length dependence of the resonant magnetoelectric effect in Ni/Pb(Zr,Ti)O3/Ni long cylindrical composites," Journal of Alloys and Compounds, vol. 615, pp. 298 – 301, 2014, doi: 10.1016/j.jallcom.2014.06.208.

[16] D. T. H. Giang, H. A. Tam, V. T. N. Khanh, N. T. Vinh, P. A. Tuan, N. V. Tuan , N. T. Ngoc, N. H. Duc, "Magnetoelectric Vortex Magnetic Field Sensors Based on the Metglas/PZT Laminates," Sensors, vol. 20, 2020, doi: 10.3390/s20102810.

[17] K. Kuczynski, "Magnetic field sensor," utility model PL 067861, 2014, (in Polish), [Online] Available: https://pl.espacenet.com/publicationDetails/biblio?II=0&ND=3&adjacent=true&locale=pl_PL&FT=D&date=20141027&CC=PL&NR=121952U1&KC=U1#.

[18] K. Kuczynski, "Possibilities of the application of hybrid magneto-piezoelectric junction as the magnetic field sensor," Przeglad Elektrotechniczny, vol. 86, no. 4, pp. 69-71, 2010 (in Polish).

[19] Catalog Ferroperm Piezoceramics A/S.

[20] K. Kuczynski, A. Bilski, P. Bilski, J. Szymanski, "Analysis of the Magnetoelectric Sensor Usability for the Energy Harvesting," International Journal of Electronics and Telecommunications, vol. 66, no. 4, pp. 787-792, 2020, doi: 10.24425/ijet.2020.135193.

[21] S. Bansal, S. Ali, G. Kapoor and R. N. Shaw, "Fourier Transform-Based Wavelet Approach for D-STATCOM Compensated Distribution Networks Fault Detection and Fault Time Computation," 2021 IEEE 4th International Conference on Computing, Power and Communication Technologies (GUCON), 2021, pp. 1-6, doi: 10.1109/GUCON50781.2021.9573674.